EVALUATION OF MODE I AND MODE II INTERFACIAL FRACTURE TOUGHNESS AND MATRIX TOUGHNESS IN FRP BY USING REAL-SIZE MODEL COMPOSITES

K. Koiwa[1*], H. Tanaka[2], Y. Nakai[2], S. Ito[2], T. Tsukahara[2], M. Bonde[2]

[1]*Nagoya institute of technology/Japan, Gokiso-tyo, Showa-ku, Nagoya*
[2]*Kobe University/Japan, 1-1 Rokkodai, Nada, Kobe*
**kozo.koiwa@nitech.ac.jp*

Keywords: Interface fracture toughness, Model composite, FRP

Abstract
Model composite methods for evaluating Mode I and Mode II fiber/matrix interfacial fracture toughness was proposed, where thin glass fibers were bonded by resin. The diameter of fibers was from 10 to 15 μm. For Mode I test, the fracture toughness tests were conducted by using model composite specimens, those were consisted of two parallel fibers, or four parallel fibers arranged in square. The fracture toughness, G_c, obtained by using the 4-fibers model composite was higher than the interfacial fracture toughness, G_i, obtained from the 2-fibers model composite. Using the values of G_c and G_i, and the fraction of the fracture surface generated by the fiber/resin debonding in the 4-fibers model composites, the resin fracture toughness in FRP was estimated on the basis of the rule of mixture. For Mode II tests, the fracture toughness tests were conducted by using Double Shear type model composite method, using 3-fibers, was proposed. By this method, Mode II interfacial fracture toughness could be evaluated, however, it depended on the resin length because of the large scale yielding at the crack tip.

1 Introduction

Recently, meso mechanical analysis was proposed to evaluate the crack propagation behavior of fiber-reinforced plastics (FRP) [1]. In this method, the macroscopic crack propagation in FRP was evaluated from the microscopic fracture process, like fiber/matrix interfacial cracking and matrix fracture [2-4], and found that the crack propagation behavior in FRP is strongly affected by the fiber/matrix interfacial debonding behavior [5, 6], while a little studies have been conducted on the fiber/matrix interfacial fracture toughness without accompanying resin fracture [7-10]. Koiwa et al. proposed a model composite method to evaluate fiber/matrix interfacial fracture toughness and matrix toughness in FRP by using two or four glass fibers from 200 to 400 μm in diameter; those were bonded by resin [9]. To evaluate the fiber/matrix interfacial fracture toughness and matrix toughness of actual FRP, the model composite method should be applied to thin fibers with diameter about 10 μm.
In the present study, the interfacial fracture toughness under different loading modes was evaluated by using glass fibers of 10 to 15 μm in diameters; those were the Double Cantilever Beam (DCB) method for Mode I, which was consisted of two fibers, and novel method called Double Shear method for Mode II, which was consisted of three fibers. To evaluate the matrix toughness in FRP in Mode I, test was also conducted by using model composite which was

consisted of four parallel glass fibers arranged in square.

2 Material and experimental procedure

2.1 Model composite specimen

Schematics of crack in FRP and model composite are shown in Figure 1. Crack propagation in bulk FRP is often along the interface between fiber and in the matrix resin associated with resin fracture as shown in Figure 1 (a). Figure 1 (b) illustrates model composite that is proposed to essentialize the fiber/matrix interfacial crack propagation behavior in bulk FRP. In the model composite, crack can propagate along the fiber/matrix interface without resin fracture. Figure 1 (c) shows another type model composite to evaluate the resin matrix toughness of FRP. In this model, crack propagates along the fiber/matrix interface and in the matrix.

In the present study, E-glass fibers of 10 to 15 μm in diameters, whose surface was treated by acrylic-silane, were employed. Surface treatments were conducted for the glass fibers by using 3-methacryloxy-propyl trimethoxysilane coupling (re-treated fiber) for reinforcing interface strength. Unsaturated polyester resin was employed for the matrix. Cobalt naphthenate (0.3 mass%) was employed as an accelerator, and Methyl ethyl ketone (2 mass%) was used as a hardener.

Schematics of the model composite are shown in Figure 2 (a) and (b), and the scanning electron micrograph of the model composite is shown in Figure 2 (c). The region where the fibers were not bonded with the resin was assumed to be an initial crack.

The fiber distance of the 2-fibers model and the 4-fibers model, δ, was about 3 μm and about 5 μm, respectively, as shown in Figure 2 (c). The central angle of fibers for the bonding region, 2θ, which is defined in Figure 2 (a), was from 60 to 120 degrees.

2.2 In-situ testing system

Mode I and Mode II in-situ tests were carried out with a special low-load-capacity tensile and compression testing machine which was installed in an inverted microscope. Figure 3 shows a schematic of the testing system.

2.3 Mode I and Mode II Interface fracture test method

Mode I tests were carried out by using DCB specimens. In Mode I test, force was applied through metal wires with diameter of 80 μm, which was bonded to fibers of the model

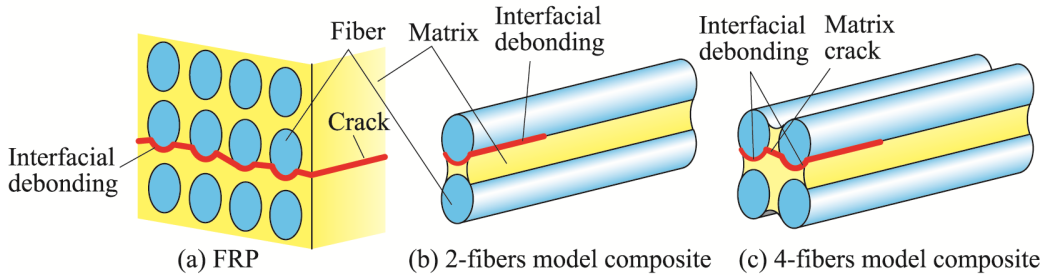

Figure 1. FRP and model composites.

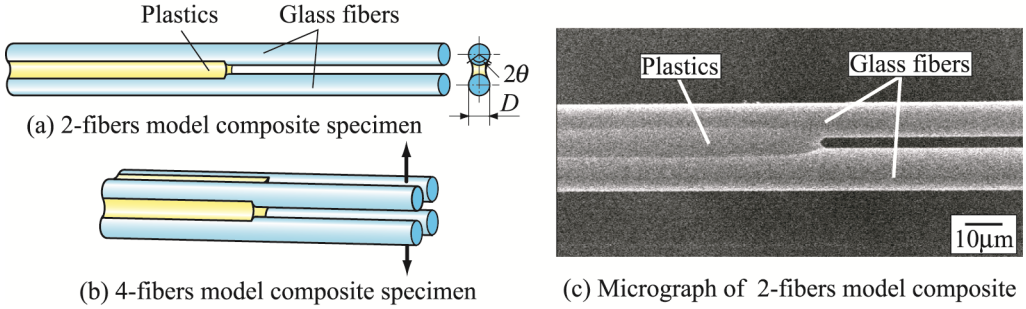

Figure 2. 2-fibers and 4-fibers model composites.

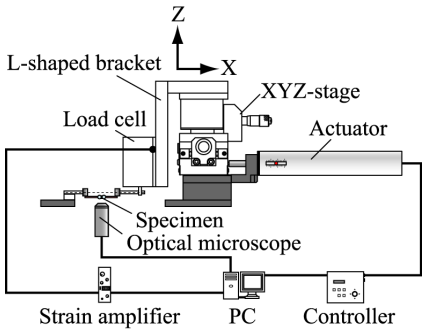

Figure 3. Schematic of Mode I and Mode II testing system.

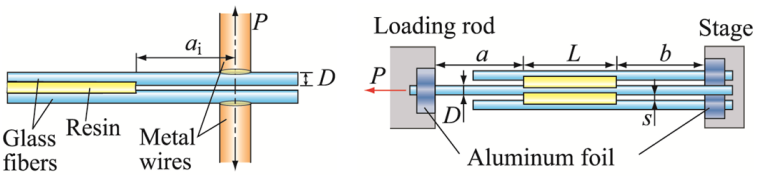

(a) Mode I specimen (b) Mode II specimen

Figure 4. Mode I and Mode II model composite specimen.

composite as shown in Figure 4 (a). The crack length, a, was from 120 to 950 μm, which was defined as the distance between the edge of bonding and the center line of the metal wire.
Mode II tests were carried out by using Double Shear specimen, as shown in Figure 4 (b). In this method, three parallel fibers were bonded by resin. Ligament length, L, fibers distance, s, crack lengths, a and b were as follows, L: 70-301 μm, s: 3.2-9.0 μm, a: 638-4530 μm, and b: 1640-4305 μm.

3 Experimental results and discussion

3.1 Mode I DCB test

3.1.1 Crack propagation behavior

Figure 5 shows the relation between applied-force and displacement for the 2-fibers and the 4-fibers DCB model composite specimens. As shown in Figure 5 (a), applied force-displacement curve of the 2-fibers model was linear before the crack initiation, and the unstable crack propagation took place just after the crack initiation because unsaturated polyester resin is brittle. As shown in Figure 5 (b), applied force and displacement curve of the 4-fibers model shows the same behavior as the 2-fibers model. Then, in case of Mode I test, the small-scale yielding condition must have been satisfied until the crack initiation.

3.1.2 Relationship between crack length and compliance

Figure 6 shows optical micrographs of deformed fibers around the loading points of the 2-fibers model composite, where the crack tips are located to the left of the photographs.
Since the fibers were not rotate with loading, the loading points are considered not to be simply supported, and bending moment must have been applied to the specimen through the loading rod. Figure 7 shows a schematic of the deformation of Mode I specimen, where Figure 7 (b) shows a model of the present study. Assuming that the loading points were not rotate, the value of compliance $\lambda=\partial\delta/\partial P$ is given by the following equations,

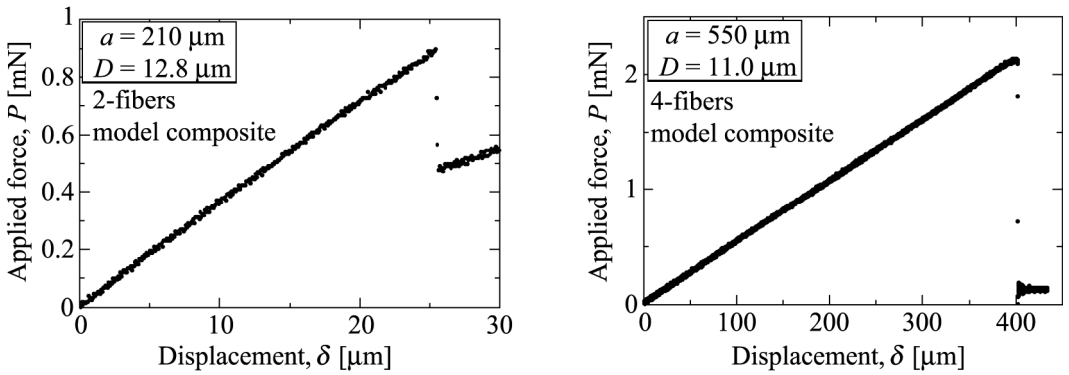

(a) 2-fibers model composite (b) 4-fibers model composite

Figure 5. Applied force – displacement curve of Mode I test.

$$\lambda = \frac{\delta}{P} = \frac{a^2}{6EI}, \quad \frac{a}{D} = \left(\frac{6EI}{D^4}\right)^{1/3} (D\lambda)^{1/3} \tag{1}$$

where E and D are Young's modulus (72.5GPa) and the diameter of glass fibers, respectively. I is the geometrical moment of inertia of fibers, which is $\pi D/64$ for the 2-fibers model and $\pi D/32$ for the 4-fibers model, respectively. In case of Figure 7 (a), the compliance is given by the following equations,

$$\lambda = \frac{\delta}{P} = \frac{2a^2}{3EI}, \quad \frac{a}{D} = \left(\frac{3EI}{2D^4}\right)^{1/3} (D\lambda)^{1/3} \tag{2}$$

Figure 8 shows the relationship between the crack length, a, and the compliance, λ. The results can be expressed as follows,

$$a/D = \alpha_0 + \alpha_1 (D\lambda)^{1/3} \tag{3}$$

where α_0 and α_1 are constants independent of the diameter and the surface treatment of fibers. The gradient of experimental results is close to that given by Equation (1), but it is much higher than that derived from Equation (2). This result indicates that Mode I specimen of present specimen was following Equation (1) in either case of the 2-fibers model and the 4-fibers model.

3.1.3Mode I interfacial fracture toughness

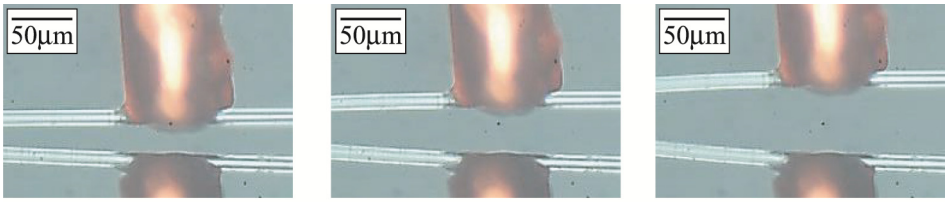

(a) P = 0.10 mN (b) P = 0.20 mN (c) P = 0.30 mN

Figure 6. Deformation of Mode I specimen (2-fibers model, a=384 μm).

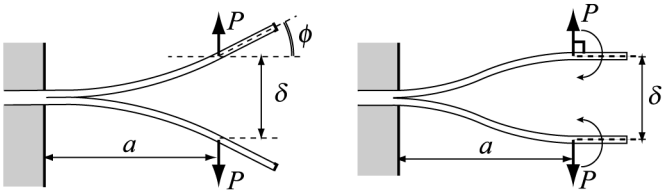

(a) DCB specimen (b) Present specimen

Figure 7. Schematic of deformation of Mode I specimen.

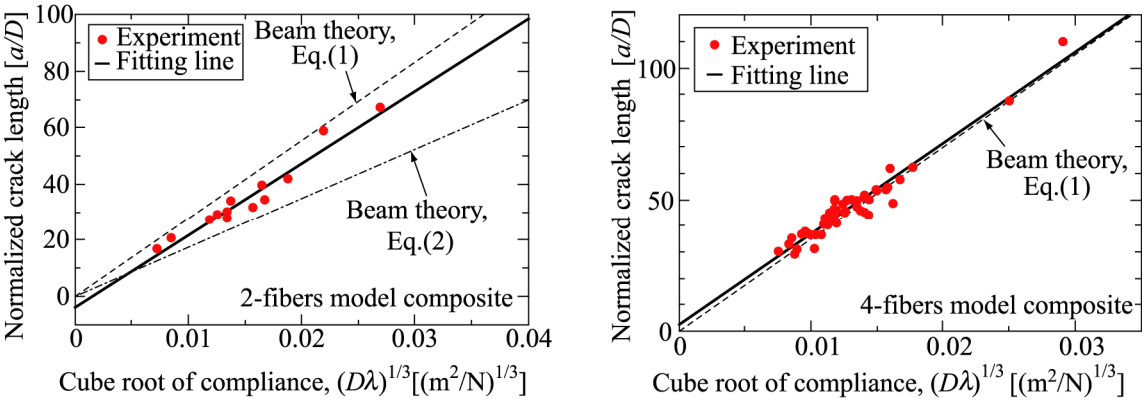

(a) 2-fiber model composite specimen (b) 4-fiber model composite specimen

Figure 8. Relation between crack length and cube root of compliance.

Figure 9 (a) and (b) show the scanning electron micrograph of fracture surface around the initial crack tips, where the upper and the lower figures are pairs of the fracture surfaces at the same specimen, and arrows in the figure indicate the crack propagation direction. Figure 9 (a) shows the fracture surface of the 2-fibers model. In the upper-side figure, there is no resin on the fracture surface, while it exists on the fiber as shown in the lower-side figure. It means that the crack propagated along the interface between fiber and resin in the 2-fibers model composite.

Figure 9 (b) shows that the crack propagation in the 4-fibers model composite was a combination of the interfacial debonding and the resin fracture as schematically shown in Figure 9 (c), where the fracture surface in the resin region was rough, and a micro crack is observed as shown by an arrow in Figure 9 (b).

The energy release rate, G, was calculated from the change of the compliance with the crack length, a, and given from Equation (3) as follows,

$$G = \frac{3P^2}{2B\theta D^3 \alpha_1^3}\left(\frac{a}{D} - \alpha_0\right)^2 \qquad (4)$$

where P is the applied-force, 2θ is the width of the bonding (see Figure 2). B is fracture surface area per unit length in the longitudinal direction of the fiber. In case of the 2-fibers model, $B=D\theta$. On the other hand, in case of the 4-fibers model, B is consisted of fracture length of interface fracture region, $D_1\theta_1+ D_2\theta_2$, and projected the length of the resin fracture perpendicular to the loading direction, L_m, then $B=D_1\theta_1+ D_2\theta_2 +L_m$ (see Figure 9 (c)).

Figure 10 shows the fracture toughness of the model composites, where the value of G_i for the 2-fibers model composite shows the pure interfacial fracture toughness of fiber/resin, and the value of G_c for the 4-fibers model composite is considered to represent the value for the actual FRP. Figure 10 (a) shows that the average value of the Mode I interface fracture toughness, G_i, was 31 J/m^2, while Figure 10 (b) show that the fracture toughness of actual FRP, G_c, was 93 J/m^2. These results indicate that the energy dissipation of the crack propagation in the actual FRP is much higher than that of the interfacial fracture.

By employing the value of the fracture toughness obtained by the 4-fibers model, G_c, and interfacial fracture toughness obtained by the 2-fibers model, G_i, and the fraction of fracture surface generated by the fiber/matrix debonding obtained by the 4-fibers model composites, the value of resin fracture toughness in FRP, G_m, was estimated on the basis of the rule of mixture by the following equation,

$$G_c = G_i\gamma_i + G_m(1-\gamma_i) \qquad (5)$$

where γ_i is the fraction of the fracture surface area of the interfacial fracture, which was given

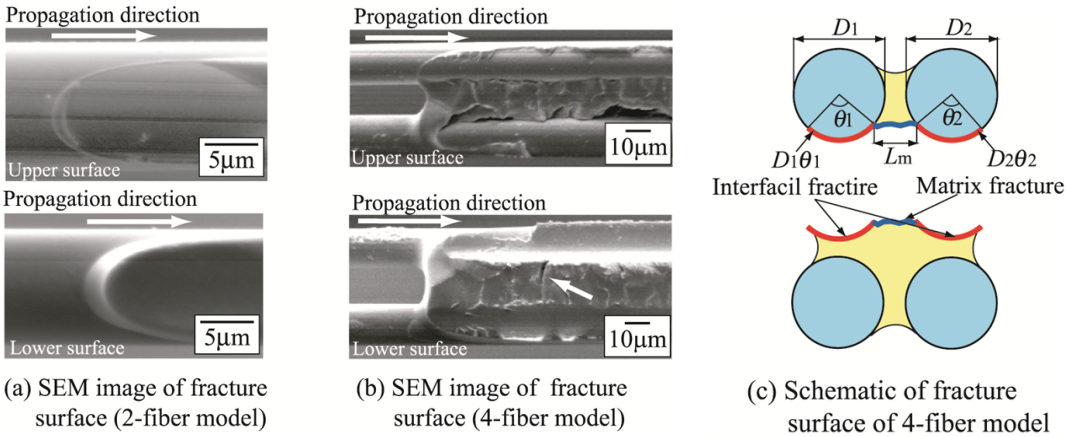

(a) SEM image of fracture surface (2-fiber model)

(b) SEM image of fracture surface (4-fiber model)

(c) Schematic of fracture surface of 4-fiber model

Figure 9. Fracture surface of Mode I specimen.

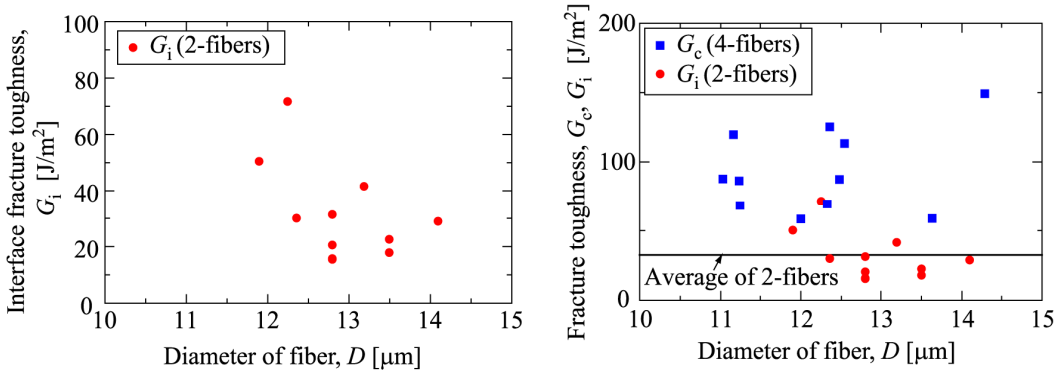

(a) 2-fibers model composeite (b) 4-fibers model composeite

Figure 10. Fracture toughness plotted against diameter of fiber.

Table 1. Average value of fracture toughness and fracture surface ratio.

	Model composite	**Unreinforced resin**
Interfacial fracture toughness, G_i (J/m^2)	31	—
Fracture toughness of 4-fibers model, G_c (J/m^2)	93	—
Fracture surface ratio of fiber/matrix debonding, γ_i	0.69	—
Estimated fracture toughness of matrix resin, G_m (J/m^2)	233	150

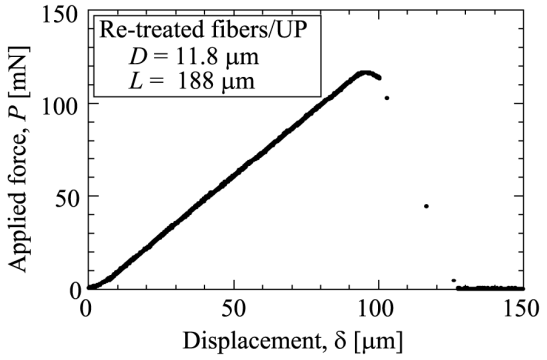

Figure 11. Applied force - displacement curve of Double Shear test.

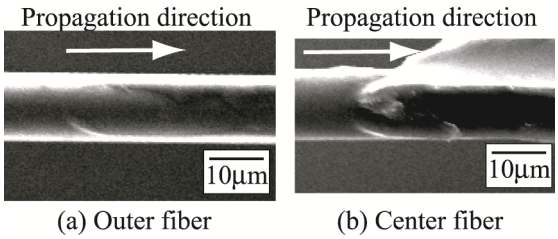

(a) Outer fiber (b) Center fiber

Figure 12. Fracture surface of specimen (outer fiber/matrix interface.

by $\gamma_i = (D_1\theta_1 + D_2\theta_2)/(D_1\theta_1 + D_2\theta_2 + L_m)$, where the experimentally obtained average value of γ_i was 0.69. The estimated value of G_m was shown in Table 1. The average of G_m is 233 J/m^2, which is much higher than the interfacial fracture toughness, G_i. This result leads that the macroscopic crack propagation of FRP tends to propagate along the interface before in resin.
The fracture toughness of resin, which was measured by using C(T) specimen made of unsaturated polyester with the width W of 24.8 mm, and the thickness B of 12.4 mm, was 150 J/m^2. This value is smaller than the value of G_m estimated by the model composites. Plastic deformation behavior of the resin around the crack tip may have been affected by fiber. Generation of micro cracks and the roughness of the fracture surface in the 4-fibers model composite also may have been responsible for the discrepancy because the fracture surface of C(T) specimen was mirror like flat plane.

3.2Mode II Double Shear test

3.2.1 Crack propagation behavior

Mode II interface fracture test were conducted by the Double Shear test. Figure 11 shows the example of the applied force-displacement relationship, where it is nonlinear in the vicinity of maximum force point because of the plastic deformation and/or the unstable crack growth.
Figure 12 shows the scanning electron micrograph of the fracture surface around the initial crack tip. On the surface of the outer fiber, no resin was attached, while it is found on the surface of the center fiber. It means that the crack propagated along the interface between the

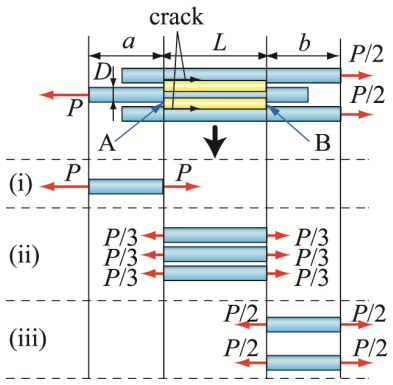

Figure 13. Simplified model of Double Shear specimen.

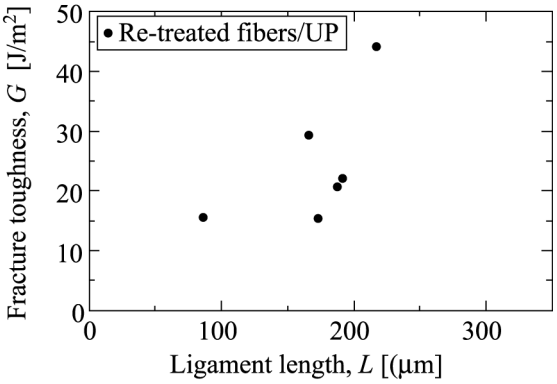

Figure 14. Relation between interface fracture toughness and ligament length.

outer fiber and the resin.

3.2.2 Energy release rate of Double Shear specimen

In the Double Shear test, the axial tensile force was applied to the fibers, and the shearing force was applied to the resin. In the present Double Shear model composite, the lengths of fibers were much longer than the lengths of bonded resin region, then, the shearing deformation of the resin is considered to be much smaller than the fiber elongation. By neglecting the effect of the shearing deformation, the energy release rate of the specimen was given by the following procedures.

From the simplified model of the Double Shear specimen as shown in Figure 13, the strain energy of the model composite is given by

$$U = U_{\mathrm{i}} + U_{\mathrm{ii}} + U_{\mathrm{iii}} \tag{6}$$

where U_{i}, U_{ii}, and U_{iii} are the strain energy of regions (i), (ii) and (iii), and given by

$$U_{\mathrm{i}} = \frac{2P^2 a}{\pi E D^2}, \quad U_{\mathrm{ii}} = \frac{2P^2 L}{3\pi E D^2}, \quad U_{\mathrm{iii}} = \frac{P^2 b}{\pi E D^2} \tag{7}$$

where E is Young's modulus of glass fiber (72.5GPa), and D is the diameter of fibers. Then, the energy release rates at the crack tips A and B are given by the following equations,

$$G_{\mathrm{A}} = \frac{1}{2\theta D}\cdot\frac{\mathrm{d}}{\mathrm{d}a}\left(U_{\mathrm{i}} + U_{\mathrm{ii}} + U_{\mathrm{iii}}\right) = \frac{1}{2\theta D}\cdot\left(\frac{\mathrm{d}U_{\mathrm{i}}}{\mathrm{d}a} - \frac{\mathrm{d}U_{\mathrm{ii}}}{\mathrm{d}L}\right) = \frac{2P^2}{3\pi E D^3 \theta}$$
$$G_{\mathrm{B}} = \frac{1}{2\theta D}\cdot\frac{\mathrm{d}}{\mathrm{d}b}\left(U_{\mathrm{i}} + U_{\mathrm{ii}} + U_{\mathrm{iii}}\right) = \frac{1}{2\theta D}\cdot\left(\frac{\mathrm{d}U_{\mathrm{iii}}}{\mathrm{d}b} - \frac{\mathrm{d}U_{\mathrm{ii}}}{\mathrm{d}L}\right) = \frac{P^2}{6\pi E D^3 \theta} \tag{8}$$

Since the value of G_{A} is higher than that of G_{B}, cracks are considered to usually initiate the at crack tip A. This is consistent with the experimental results.

3.2.3 Mode II interface fracture toughness

As shown in Figure 14, the interfacial fracture toughness obtained by the Double Shear tests depended on the ligament size, L. It may have come from the large scale yielding; then, the elastic-plastic fracture mechanics approach should be conducted.

4 Conclusions

New test methods using model composites, Double Cantilever Beam (DCB) for Mode I and Double Shear specimens for Mode II, were proposed, and the following results were obtained.

(1) In Mode I test of the model composites consisted of two or four fibers and unsaturated polyester resin, the interfacial fracture toughness, G_{i}, and the fracture toughness of FRP, G_{c}, which included matrix toughness, could be evaluated, and the value of G_{c} was three

times higher than the value of G_i because of the high energy dissipation by the matrix fracture.

(2) By employing the values of G_i, G_c, and the fracture surface ratio of fiber/matrix debonding in the 4-fibers model composites, the matrix fracture toughness in FRP, G_m, was estimated on the basis of the rule of mixture. The estimated value of G_m was higher than that of the bulk unsaturated polyester. It may have been be responsible to the high roughness of the fracture surfaces in FRP, and the difference in resin deformation behavior between bulk resin and FRP.

(3) In Mode II test, new test method "Double Shear" by using 3-fibers model composite was proposed. In this test, however, valid fracture toughness value could not be obtained from the linear elastic fracture mechanics. To evaluate the valid Mode II fracture toughness, non-linear fracture mechanics approach should be developed.

References

[1] Friedrich K., Fractographic Analysis of Polymer Composites, *Composite Materials* **Series 6,** Application of Fracture Mechanics to Composite Materials, pp. 425-487, Elsevier Science. (1989).

[2] Crews, J.H., Jr., Shivakumar, K.N. and Raju, I.S. A Fibre-Resin Micromechanics Analysis of the Delamination Front in a Double Cantilever Beam Specimen, *Phase Interaction in Composite Materials*, pp. 396-405, Omega Scientific, (1992).

[3] Dubois, F. and Keunings, R. DCB Testing of Thermoplastic Composites: A Non-Linear Micro-Macro Numerical Analysis, *Composites Science and Technology*, **Vol. 57**, No. 4, pp. 437-450, (1997).

[4] Tanaka H. and Nakai Y. Three-Dimensional Micromechanics Analysis of Strain Energy Release Rate Distribution along Delamination Crack in FRP, Composites Technologies for 2020, Proceedings of the 4th Asian-Australasian Conference on Composite Materials, pp. 439-444, Woodhead Publishing Ltd, (2004).

[5] Kotaki M., Hojo M., Tsujioka, N. and Hamada H. Effect of Surface Treatment on Interlaminar/Intralaminar Crack Growth Behavior of CFRP Laminates, Proceedings of the 4th Japan International SAMPE Symposium, pp. 1008-1013, (1995).

[6] Hojo M., Tsujioka N., Kotaki M., Hamada H., Maekawa, Z. and Ochiai, S., "Effect of Interfacial Strength on Interlaminar and Intralaminar Fracture Toughness of CFRP Laminates", High Technology Composites in Modern Applications, Proceedings of *COMP'95*, pp. 30-36, (1995).

[7] Hojo M., Tanaka M., Hobbiebrunken T., Ochiai S., Inoue T. and Sawada Y. Interfacial Fracture of GF and CF/Epoxy Model Composites under Static and Fatigue Loadings, Proceedings of *the 8th International Fatigue Congress*, Fatigue 2002, pp. 231-238, EMAS, (2002).

[8] Tanaka M., Kawaguchi T., Hojo M., Ochiai S. and Nakanishi Y. In-situ Observation of Interfacial Debonding Process Induced by Matrix Crack Propagation in Two-Dimensional Unidirectional Model Composites, *Composite Interfaces*, **Vol. 15**, No. 1, pp. 75-94, (2008).

[9] Koiwa, K., Tanaka, H., Hiwa, T., Nakai, Y., "Evaluation of Fiber/Matrix Interfacial Fracture Toughness and Its Contribution to Composite Toughness by Using Two and Four-Fibers Model Composite Specimens", Journal of the Society of Material Science Japan, **Vol. 57**, No. 12, pp. 1205-1211, (2008).

[10] D.J. Wilkins, J.R. Eisenmann, R.A. Camis, W.S. Margolis and R.A. Benson, "Characterizing delamination growth in graphite-epoxy", *Damage in Composite Materials*, ASTM Special Technical Publication 775, pp. 168-183 American Society for Testing and Materials, Philadelphia, (1982).